


Research Article

Open Access



# All 3D-printed high-sensitivity adaptive hydrogel strain sensor for accurate plant growth monitoring

Lina Wang<sup>1,2,#</sup>, Wen Wang<sup>1,#</sup>, Rongtai Wan<sup>1,2,#</sup>, Mutian Yao<sup>1,2</sup>, Wenna Chen<sup>2</sup>, Liuyu Zhang<sup>3</sup>, Jingkun Xu<sup>1</sup>, Ximei Liu<sup>1,2,\*</sup>, Baoyang Lu<sup>1,2,\*</sup> 

<sup>1</sup>Jiangxi Provincial Key Laboratory of Flexible Electronics, Jiangxi Science and Technology Normal University, Nanchang 330013, Jiangxi, China.

<sup>2</sup>School of Pharmacy, Jiangxi Science and Technology Normal University, Nanchang 330013, Jiangxi, China.

<sup>3</sup>College of Information Science & Engineering, Shenyang Ligong University, Shenyang 110159, Liaoning, China.

# Authors contributed equally.

\* **Correspondence to:** Prof. Ximei Liu, School of Pharmacy, Jiangxi Science and Technology Normal University, No. 605 Fenglin Avenue, Changbei Economic Development Zone, Nanchang 330013, Jiangxi, China. E-mail: liuxm@jxstnu.edu.cn; Prof. Baoyang Lu, Jiangxi Provincial Key Laboratory of Flexible Electronics, Jiangxi Science and Technology Normal University, No. 605 Fenglin Avenue, Changbei Economic Development Zone, Nanchang 330013, Jiangxi, China. E-mail: luby@jxstnu.edu.cn

**How to cite this article:** Wang, L.; Wang, W.; Wan, R.; Yao, M.; Chen, W.; Zhang, L.; Xu, J.; Liu, X.; Lu, B. All 3D-printed high-sensitivity adaptive hydrogel strain sensor for accurate plant growth monitoring. *Soft Sci.* 2025, 5, 2. <https://dx.doi.org/10.20517/ss.2024.38>

**Received:** 5 Sep 2024 **First Decision:** 22 Oct 2024 **Revised:** 18 Nov 2024 **Accepted:** 21 Nov 2024 **Published:** 16 Jan 2025

**Academic Editors:** Toan Dinh, YongAn Huang **Copy Editor:** Pei-Yun Wang **Production Editor:** Pei-Yun Wang

## Abstract

Highly sensitive strain sensors are crucial for monitoring subtle plant growth changes and show diverse applications in plant sensing. However, the prevailing integrated fabrication methods for such sensors tend to be costly and complex, impeding their fundamental design and practical usage. Herein, we develop a simple and effective multimaterial all-3D printing technique to manufacture integrated strain sensors with a multilayered structure. Such an all-3D-printed strain sensor exhibits excellent sensing performance enabling precise detection of minor strains in plant growth, including high stretchability (> 300%), high sensitivity (~12.78) with good linearity (0.98), and good long-term stability over 3,000 loading/unloading cycles. We further validate the potential applications of our 3D-printed integrated strain sensor for accurate and continuous monitoring of bamboo growth in both horizontal and vertical directions over 14 days. Our all-3D-printed strain sensor offers a promising avenue for integrated strain sensing systems toward plant growth monitoring.

**Keywords:** Hydrogel strain sensor, 3D printing, high sensitivity, plant growth monitoring



© The Author(s) 2025. **Open Access** This article is licensed under a Creative Commons Attribution 4.0 International License (<https://creativecommons.org/licenses/by/4.0/>), which permits unrestricted use, sharing, adaptation, distribution and reproduction in any medium or format, for any purpose, even commercially, as long as you give appropriate credit to the original author(s) and the source, provide a link to the Creative Commons license, and indicate if changes were made.



## INTRODUCTION

Global climate change and viral pests have severely affected crop yields, posing a major threat to the global food supply. Ensuring sustainable growth in crop yield is crucial to addressing food shortages. Achieving this goal requires comprehensive understanding of the biological and environmental factors that influence plant growth, which play a key role in improving crop yield<sup>[1]</sup>. Strain sensors offer a technique to monitor plant growth by detecting external deformations in plant structures. However, many existing plant strain sensors suffer from several limitations, including restricted tensile properties and high mechanical strength, which can affect or even damage plant tissues during practical use<sup>[2]</sup>. Hydrogel-based strain sensors, known for their soft stretchability, provide non-damaging, long-term, real-time monitoring, and have found wide applications in fields such as healthcare<sup>[3-5]</sup>, soft robotics<sup>[6-8]</sup>, and wearable electronics<sup>[9-14]</sup>. Despite these advancements, current strain sensors still face challenges related to interface compatibility and programmability. They are often constructed from thin films with varying structures<sup>[15,16]</sup> or 3D-printed sensing layers on flexible substrates<sup>[17,18]</sup>. These issues result in unstable signals, insufficient measurement accuracy, and complex fabrication processes, which limit their ability/stability to adapt to dynamic environmental conditions and evolving application needs. Although progress has been made to overcome these challenges, the design and fabrication of integrated sensing devices that combine simple manufacturing processes with high sensitivity remains a significant hurdle.

Hydrogel strain sensors are typically designed with sandwich structures comprising a substrate, a sensing layer, and an encapsulation layer, each with a thickness of a few hundred micrometers<sup>[19-22]</sup>. However, integrating these layers often involves complex processes, such as spin-coating the substrate<sup>[23,24]</sup>, screen-printing<sup>[25]</sup>, etching<sup>[26,27]</sup>, spraying<sup>[28-30]</sup>, and cutting the encapsulation layer. These procedures are intricate, requiring expensive equipment and manual assembly, which can weaken the interface between components and limit the structural flexibility of the device. Such limitations primarily restrict designs to planar structures, thereby constraining the overall functionality of the device<sup>[31,32]</sup>. To address these challenges, 3D printing has emerged as a promising technique solution for overcoming the complexity of traditional sensor fabrication<sup>[33-35]</sup>. Various 3D printing techniques, including digital light processing (DLP)<sup>[36-39]</sup>, stereolithography<sup>[40]</sup>, and direct ink writing (DIW)<sup>[41-43]</sup>, have been explored and widely adopted for customizable sensor manufacturing. Among them, DIW is considered as the most straightforward 3D printing technology owing to its unique advantages free of external factors such as light or heat, and no additional non-functional material components (e.g., photosensitive monomers), making it particularly suitable for fabricating integrated sensor devices. In contrast to the equipment and process limitations of traditional manufacturing methods in creating complex shapes, 3D printing technology enables the customization of sensor structures during the design phase. By fine-tuning the sensor's geometry, 3D printing can address certain geometric imperfections or errors, minimizing signal deviations due to external deformations and ensuring stable output across diverse strain conditions<sup>[44]</sup>. However, achieving repeatable and programmable 3D printing of strain sensors remains a challenge. Successful 3D printing of strain sensing devices with DIW requires high-performance yet stable ink materials, ink rheology optimization<sup>[45]</sup>, printing parameter adjustment, shape fidelity improvement, and multilayer interface integration.

Herein, we successfully fabricate integrated strain sensors for real-time monitoring of plant growth using multi-material 3D printing [Figure 1A]. Various strain sensors with different structures are designed and explored to reveal the structure-performance relationship and enhance the sensitivity under the same strain conditions. Additionally, we carefully optimize the printing parameters for two types of inks: a viscous polyvinyl alcohol (PVA) solution and a conductive poly(3,4-ethylenedioxythiophene):polystyrene sulfonate (PEDOT:PSS)-PVA ink. This meticulous optimization ensures precise ink deposition, reduces diffusion, maintains shape fidelity, and seamlessly integrates multiple materials. Meanwhile, we prove the printability

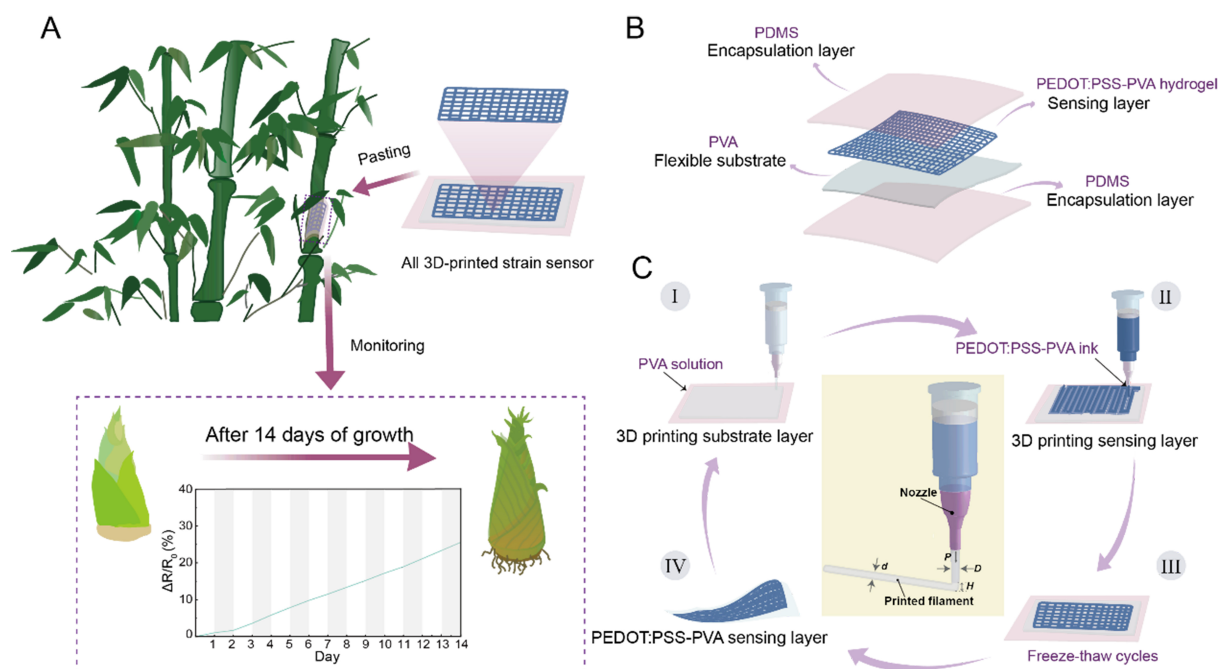


**Figure 1.** Design of an integrated 3D printing strain sensing device. (A) Integrated 3D-printed strain sensing device for plant growth monitoring; (B) Schematic diagram of the multi-material structure of the strain sensing device. The integrated device contains a four-layer structure: PDMS substrate layer, PVA flexible substrate layer, PEDOT:PSS-PVA sensing layer, and PDMS encapsulation layer; (C) Printing process of integrated strain sensor devices. PDMS: Polydimethylsiloxane; PVA: polyvinyl alcohol; PEDOT:PSS: poly(3,4-ethylenedioxythiophene):polystyrene sulfonate.

of multi-material inks using DIW-based 3D printing and indicate that the printed sensors keep a tight interface between the substrate layer and the sensing layer. Finally, our experimental results demonstrate that the 3D-printed square sensing device shows the highest sensitivity [gauge factor (GF) = 12.78] compared to other structures. Furthermore, we evaluate potential applications of such a 3D-printed integrated sensing device for continuous accurate monitoring of bamboo growth in both horizontal and vertical directions over 14 days.

## EXPERIMENTAL

### Materials

PEDOT:PSS (Kaivo, Zhuhai), PVA (Mw: 124000-186000 Da, Sigma-Aldrich), 184 silicone elastomer [polydimethylsiloxane (PDMS), 0008912877], 184 silicone elastomer curing agent (PDMS curing agent, H052J9A063), and dimethyl sulfoxide (DMSO, > 99.8%, Aladdin, Shanghai) were purchased and directly used without further purification. Milli-Q purified water was employed for all experiments.

### Preparation of 3D printable inks

**Preparation of PEDOT:PSS-PVA ink:** PEDOT:PSS nanofibrils (0.6 g) were re-dispersed with a DMSO-deionized water mixture (9.4 g, DMSO: deionized water = 15:85 v/v) to prepare 6 wt.% PEDOT:PSS solution. Then, 6 g PVA was added to 44 g deionized water to prepare 12 wt.% PVA dispersion solution (stirred at 90 °C for 2 h until completely dissolved). The 3D printable PEDOT:PSS-PVA ink was prepared by mixing the above 6 wt.% PEDOT:PSS solution and 12 wt.% PVA solution in a ratio of 1:2, and then degassed with a centrifuge at 8,000 rpm for 5 min.

Preparation of PVA ink: PVA (6 g) was added to 44 g deionized water to prepare 12 wt.% PVA dispersion solution (stirred at 90 °C for 2 h until completely dissolved).

Preparation of PDMS ink: PDMS ink was obtained by mixing the PDMS curing agent with the PDMS precursor solution in a ratio of 1:10 and stirring under mechanical agitation for 20-30 min to obtain a homogeneous mixture and centrifuging to remove air bubbles. To prevent rapid curing of PDMS, PDMS inks need to be dispensed as they were used.

### 3D printing of integrated strain sensor devices

The optimization of printing parameters for PEDOT:PSS-PVA and PVA inks, and the 3D printing of the integrated strain sensing device were carried out on a DB-100 3D printer (Shanghai Mifang Electronic Technology Co., Ltd., Shanghai, China). The structures of all 3D printed layers were drawn using Adobe Illustrator 2021 software and saved in a scalable vector graphics (SVG) format. The printing process was carried out by using varying printing needles with diameters of 90, 160, 210, 260, 340, and 410  $\mu\text{m}$ , with printing air pressure selections of 50, 100, 150, 200, 250, and 300 kPa, and printing speed adjustments of 0-8  $\text{mm}\cdot\text{s}^{-1}$ . Before starting the printing process, the printed layer structures in an SVG format were imported into the DB-100 software, and the model was further adjusted to fit the printer [Supplementary Figure 1]; then, the printing parameters were set according to the requirements. First, we printed the PDMS encapsulation layer and the PVA substrate layer, followed by the PEDOT:PSS-PVA hydrogel sensing layer. Then, we attached the wires to the sensing layer. Finally, we printed the topmost PDMS encapsulation layer. After printing, the PDMS layer was cured at room temperature, while the PVA and PEDOT:PSS-PVA layers underwent three cycles of freezing at -20 °C for 8 h and thawing at 25 °C for 3 h.

### Characterizations

Scanning electron microscope (SEM) images of the PVA layer at the interface with the PEDOT:PSS-PVA layer were acquired by a SEM (TESCAN). Viscosity versus shear rate of PEDOT:PSS-PVA and PVA hydrogel was performed by a Discovery Hybrid rheometer (TA Instrument) with a 40 mm diameter flat plate geometry at 25 °C. Shear rates are ranged from 0-400  $\text{s}^{-1}$ .

### Mechanical measurements

A microcomputer-controlled universal testing machine (ZQ-990LB, ZHIQU Precision Instruments) was used to perform the mechanical properties of PEDOT:PSS-PVA (grid structure) and PVA [25 mm (length)  $\times$  2.5 mm (width)  $\times$  1 mm (thickness)] hydrogel at a constant tensile speed of 100  $\text{mm}\cdot\text{min}^{-1}$ . The Young's modulus of PEDOT:PSS-PVA and PVA hydrogel can be calculated from the stress-strain curve and the toughness was calculated from the integrated area of stress-strain.

### Electrical measurements

To measure the electrical conductivity, the resistance of PEDOT:PSS-PVA hydrogels was recorded by a Keithley 2700 digital multimeter based on a conventional four-point probe method. The width and length of the sample were measured by a Vernier caliper, and the thickness of the samples was using a screw micrometer. The electrical conductivity ( $\sigma$ ) of all the hydrogel samples was calculated according to:

$$\sigma = L/WRT$$

where  $L$ ,  $W$ ,  $R$ , and  $T$  are the length, width, resistance, and thickness of the samples, respectively.

### Sensing performance measurements

The sensing performance of the one-piece 3D printed device was tested using an LCR (Tonghui, TH2829C) instrument. The sensing signals were tested at different strains, i.e., 50%, 100%, 150%, 200%, 250%, and 300%. The sensitivity of the hydrogel strain sensors was determined by analyzing the changes in the sensed signals at different strains, and the sensitivity (GF) was calculated using:

$$GF = \Delta R / (R_0 \times \varepsilon)$$

where  $\Delta R$  is the change in resistance,  $R_0$  is the original resistance,  $\varepsilon$  is the sensor strain.

## RESULTS AND DISCUSSION

### Design of 3D printing PEDOT:PSS-PVA strain sensing device

We aim to simplify the fabrication process of customized strain sensing devices for integrated continuous multi-material production, eliminating any manual or tedious processes. To achieve this, we propose a novel all-3D-printing method based on DIW technology to achieve integrated device manufacturing. Leveraging the unique properties of 3D printing, we design a four-layered overlapping structure for the sensing device through continuous printing. To ensure seamless integration of interfaces during the multi-material printing process, we extensively investigate the printability of different viscoelastic inks. Based on quantified results, we select the optimal printing parameters for each functional layer material to manufacture strain-sensing devices with programmable, continuous, and seamless interfaces.

We have designed a four-layer stacked structure for the strain sensing device, consisting of the base layer, flexible substrate, conductive layer, and encapsulation layer [Figure 1B]. The device is fabricated by sequentially printing multiple materials with different functionalities [Figure 1C]. Initially, we use PDMS as a supporting film due to its hydrophobicity and long-term stability. Next, a soft, highly stretchable PVA film serves as the flexible substrate. Then, a conductive hydrogel layer of multilinear conductive PEDOT:PSS-PVA ink is continuously printed onto the PVA substrate. To address potential issues such as water loss or absorption, a PDMS film is printed on top of the conductive and flexible substrate layers as a protective encapsulation. Interestingly, the PEDOT:PSS-PVA sensing layer integrates seamlessly with the PVA flexible substrate, effectively reducing interlayer slip. This tight integration is primarily due to the interaction between PEDOT:PSS and PVA. As illustrated in Supplementary Figure 2, the PEDOT semi-crystalline domains and PVA crystalline domains are physically cross-linked after undergoing continuous freeze-thawing cycles, forming a stable microphase semi-separated network. Mechanistically, multiple interactions within the hydrogel matrix - including entanglements between PSS and PVA chains, hydrogen bonding between PVA chains, and electrostatic interactions between PVA/PSS and PEDOT - play a significant role in enhancing the interfacial stability of the device, ensuring stable and reliable sensing signal output<sup>[46,47]</sup>.

### Optimization of 3D printing parameters for multi-material inks

The integrated 3D-printed strain sensing device consists of encapsulation layers (PDMS elastomer), a strain sensing functional layer (PEDOT:PSS/PVA hydrogel), and a substrate layer (PVA hydrogel). The integrated 3D printing of multilayer structures is a complex process requiring collaborative optimization. To ensure accurate, high-precision printing integration, we minutely optimize the printing parameters of the strain-sensing functional layer and the substrate layer, including nozzle size, printing pressure, and printing speed. The viscosity of PEDOT:PSS-PVA ink is firstly characterized by the shear rate as the rheological properties of the ink are crucial for 3D printability. The ink exhibits robust shear-thinning behavior, maintaining its shape after the extrusion process. At the same time, a high yield stress prevents the printed structure from collapsing before cross-linking [Supplementary Figure 3].

Moreover, fine tuning of 3D-printable inks is crucial for ensuring the integrity and precision of the devices. To guarantee proper adhesion between layers and optimize the structure of the sensing layer, we investigate the shape fidelity of the ink under various conditions, including printing pressure, nozzle diameter, and printing speed. During the 3D printing process, smaller nozzles and lower printing pressures may lead to issues such as print failures, discontinuous lines, and poor shape fidelity. In contrast, larger nozzles and higher printing pressures can cause the ink lines to extend beyond the nozzle diameter or spread on the substrate, resulting in poor shape fidelity.

Based on these issues, we conduct a detailed study on PEDOT:PSS-PVA conductive ink and PVA ink. First, we print PEDOT:PSS-PVA conductive ink and evaluated its printability under fixed printing speed ( $1 \text{ mm}\cdot\text{s}^{-1}$ ), varying nozzle sizes ( $90\text{--}410 \text{ }\mu\text{m}$ ), and printing pressures ( $50\text{--}300 \text{ kPa}$ ), as displayed in [Figure 2A](#). By optimizing printing pressure and nozzle size, we further investigate the effect of printing speed on the printability of the conductive ink. When the nozzle size is fixed at  $210 \text{ }\mu\text{m}$ , the printing speed for PEDOT:PSS-PVA conductive ink has been found to range from  $0.5$  to  $6 \text{ mm}\cdot\text{s}^{-1}$  [[Figure 2B](#)]. For a fixed nozzle size of  $260 \text{ }\mu\text{m}$ , the printing speed ranged from  $0.5$  to  $8 \text{ mm}\cdot\text{s}^{-1}$  [[Supplementary Figure 4A](#)]. To visually assess the shape and line width of the ink during the printing process, we place the printed ink lines under a microscope for observation and recording, thereby precisely determining the ink's printing shape under different parameters [[Figure 2C](#)]. Meanwhile, we evaluate the printability of PVA ink. Under fixed printing speed ( $1 \text{ mm}\cdot\text{s}^{-1}$ ), varying nozzle sizes ( $90\text{--}410 \text{ }\mu\text{m}$ ), and printing pressures ( $50\text{--}300 \text{ kPa}$ ), the printability of PVA ink is shown in [Figure 2D](#). After optimizing the pressure and nozzle size parameters, we further investigate the impact of printing speed on the shape fidelity of the ink. When the nozzle size was fixed at  $260 \text{ }\mu\text{m}$ , the printing speed range for PVA ink was  $0.5$  to  $8 \text{ mm}\cdot\text{s}^{-1}$  [[Figure 2E](#)]. When the nozzle size was set to  $210 \text{ }\mu\text{m}$ , the printing speed range was between  $0.5\text{--}6 \text{ mm}\cdot\text{s}^{-1}$  [[Supplementary Figure 4B](#)]. Additionally, all ink parameter adjustments have been evaluated based on the extent of ink diffusion observed under electron microscopy [[Figure 2F](#)].

Through optimization of various parameters, the minimum printable resolution achieved with the  $210 \text{ }\mu\text{m}$  needle is  $237 \text{ }\mu\text{m}$  for PVA ink and  $251 \text{ }\mu\text{m}$  for PEDOT:PSS-PVA conductive ink. To ensure fast and uniform printing of the substrate layer, a  $260 \text{ }\mu\text{m}$  nozzle is used for the PVA layer at a speed of  $0.5\text{--}8 \text{ mm}\cdot\text{s}^{-1}$ . Simultaneously, a nozzle size of  $210 \text{ }\mu\text{m}$  and a printing speed of  $0.5\text{--}6 \text{ mm}\cdot\text{s}^{-1}$  ensure high-precision printing of the PEDOT:PSS-PVA layer. Therefore, by optimizing the printability parameters of multi-material inks, continuous and integrated fabrication of sensor devices can be achieved.

### 3D printing of integrated strain sensing devices

Based on the systematic optimization of PEDOT:PSS-PVA and PVA inks, the prepared inks are loaded into syringes respectively [[Figure 3A](#) and [Supplementary Movie 1](#)] and printed after carefully selecting the optimal printing parameters to ensure high fidelity of printed lines and achieve seamless interface integration during multi-material printing. Specifically, the PEDOT:PSS-PVA layer is printed using optimal 3D printing parameters ( $300 \text{ kPa}$  pressure,  $2 \text{ mm}\cdot\text{s}^{-1}$  speed,  $210 \text{ }\mu\text{m}$  needle diameter), and the PVA layer is printed with parameters of  $300 \text{ kPa}$  pressure,  $5 \text{ mm}\cdot\text{s}^{-1}$  speed, and  $260 \text{ }\mu\text{m}$  needle diameter. Subsequently, the sensing device is integrated and 3D printed with PEDOT:PSS, PVA, and PDMS inks under the optimal printing parameters [[Figure 3B](#)]. After completing the layer-by-layer printing of the device, we solidify the device to ensure seamless integration. As demonstrated in [Supplementary Figure 5](#), the SEM image indicates that the surface sensing layer and the substrate layer are closely connected, which is conducive to the stability of the interface. Additionally, utilizing the integrated 3D printing process, we design conductive layers with various structures to explore the relationship between structure and performance [[Figure 3C-I](#)], facilitating the integrated preparation of multi-structure strain sensors. Upon completing the entire 3D printing process, we conduct a comprehensive evaluation to assess the performance and feasibility of the

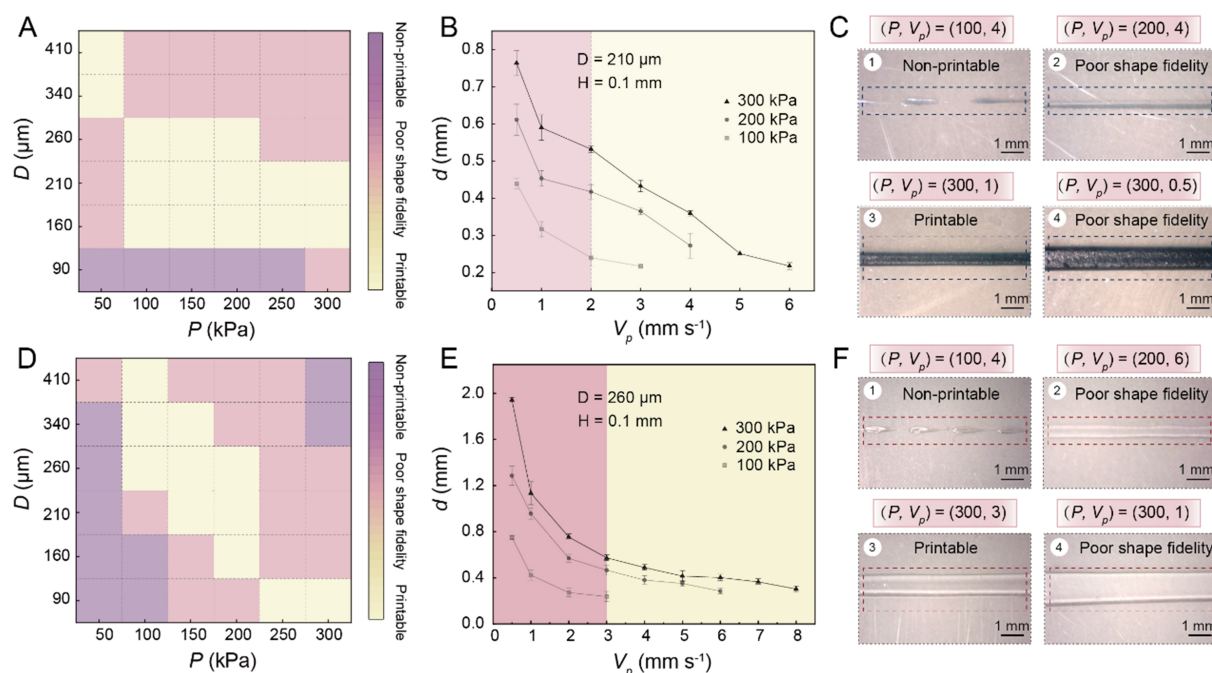


**Figure 2.** Evaluation of multi-material ink printability. (A) Phase diagram of the printability of PEDOT:PSS-PVA ink under different print nozzle sizes (90–410  $\mu\text{m}$ ) and different print pressures (50–300  $\mu\text{m}$ ); (B) Printed PEDOT:PSS-PVA ink line width vs. print speed (0–6  $\text{mm}\cdot\text{s}^{-1}$ ) and printing pressure (100, 200, 300 kPa) for the print nozzle size of 210  $\mu\text{m}$  and the print height of 0.1 mm; (C) PEDOT:PSS-PVA ink lines printed under different printing parameters; (D) Phase diagram of the printability of PVA ink under different print nozzle sizes (90–410  $\mu\text{m}$ ) and different print pressures (50–300  $\mu\text{m}$ ); (E) Printed PVA ink line width vs. print speed (0–8  $\text{mm}\cdot\text{s}^{-1}$ ) and print pressure (100, 200, 300 kPa) for the print nozzle size of 260  $\mu\text{m}$  and the print height of 0.1 mm; (F) PVA ink lines printed under different printing parameters. PEDOT:PSS: Poly(3,4-ethylenedioxythiophene):polystyrene sulfonate; PVA: polyvinyl alcohol.

sensor device, focusing on its mechanical properties and electrical and sensing performance.

Due to the physical cross-linking of PVA chains, our conductive hydrogel demonstrates high stretchability, exceeding 300% [Supplementary Figures 6 and 7]. Additionally, PEDOT:PSS, serving as the electrical phase, interweaves with PVA chains to form a conductive network with excellent mechanical properties, and as the PEDOT:PSS content increases, its conductivity rises [Supplementary Figure 8]. To systematically analyze the sensing characteristics of the integrated 3D-printed sensor device, we select PDMS as the encapsulation layer to enhance device stability. Excitingly, the hydrogel sensor encapsulated with PDMS exhibits excellent water retention and electrical signal stability; even after two days of storage, its relative resistance signal remains nearly consistent with the initial values [Supplementary Figures 9 and 10]. Moreover, we further evaluate the sensing properties of PEDOT:PSS-PVA conductive hydrogels with different structures; we have tested their relative resistance changes across various strain ranges and calculated their sensitivity values [Figure 3D–J]. The results indicate that the sensor with a square structure exhibits the highest sensitivity [Supplementary Figures 11 and 12]. At the same time, we have compared the sensing performance of the planar structure sensor under different strains and found that it has a lower sensitivity value than the square structure sensor [Supplementary Figure 13]. These results indicate that the sensor's sensitivity is closely related to its structure, and performance breakthroughs can be achieved by altering the sensing layer's structure. During the stretching process, the conductive pathways of sensors with different structures change, leading to variations in relative resistance values. As illustrated from the SEM images, the conductive path expands after stretching [Supplementary Figure 14], which in turn increases the GF. Among various structures, the square configuration exhibits the most significant change during stretching,

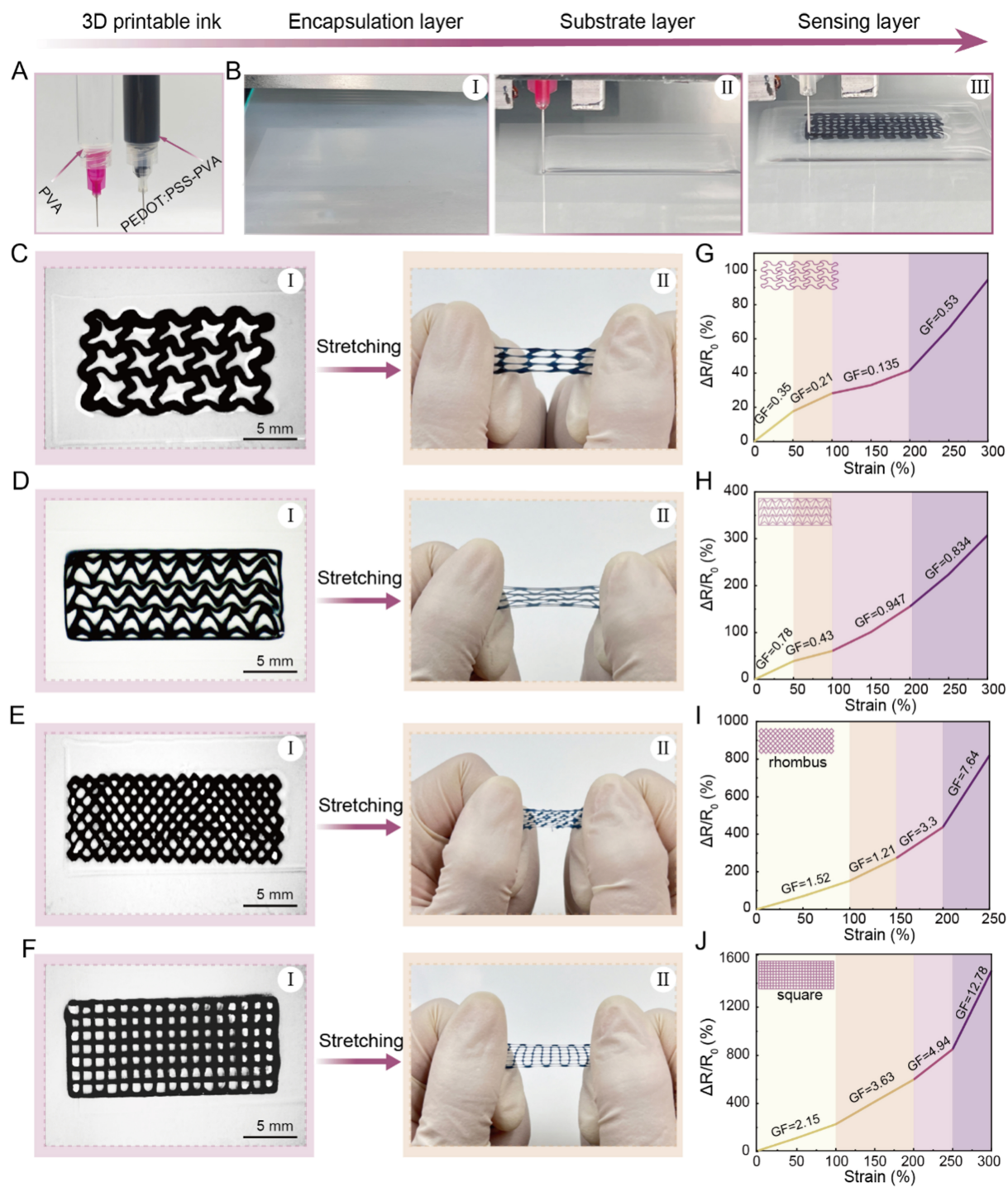


**Figure 3.** All 3D printed strain sensing devices and sensitivity analysis. (A) Physical drawing of PEDOT:PSS-PVA ink and PVA ink; (B) The 3D printing process for integrated strain sensor devices; Conductive layer structure with different patterns and stretching objects: (C) Microwave pattern; (D) Curved line; (E) Rhombic; (F) Square; Sensing performance of different shape patterns under different strains (0%-300%): (G) Microwave pattern; (H) Curved line; (I) Rhombic; (J) Square. PEDOT:PSS: Poly(3,4-ethylenedioxythiophene):polystyrene sulfonate; PVA: polyvinyl alcohol.

resulting in larger resistance change per unit strain, thereby improving the sensitivity. Additionally, microcracks play a crucial role in influencing the sensor's sensitivity. When the applied stress exceeds the

fracture threshold, the conductive path is interrupted, causing a significant change in resistance<sup>[48,49]</sup>. As illustrated in [Supplementary Figure 15](#), crack propagation in the conductive path of the square structure is more pronounced under stretching, leading to a substantial increase in resistance and enhancing the sensor's sensitivity. This 3D printing strategy significantly enhances the tunability of the sensing layer's structure, thereby boosting the sensor's sensitivity and enabling the customized design of sensor devices.

### **Sensing properties of the 3D printed PEDOT:PSS-PVA strain sensing device**

Due to the sensitivity analysis of sensors with different structures, we found that the square structure device exhibits a higher sensitivity value. Therefore, we systematically explored various performance parameters of the square sensor, including hysteresis, linearity, response time, and stability. Leveraging the high mechanical properties of the PEDOT:PSS-PVA hydrogel, our integrated printed strain sensor demonstrated a stable response to cyclic loads under different tensile states. The prepared sensor can detect relative resistance signal changes within a large strain range (0%-300%), medium strain range (0%-100%), and a really small deformation range (0%-30%) [[Figure 4A](#) and [Supplementary Figure 16](#)]. The resistance signals showed a stable gradient change after multiple loading and unloading cycles at different strains, with cyclic resistance values remaining stable, indicating the device's reusability at specific strains. Surprisingly, the device maintained a linearity of 0.98 at strains up to 300%, demonstrating its ability to reflect actual changes more stably and accurately during measurements. Additionally, our sensor exhibits low hysteresis (< 0.4%), enabling precise detection of resistance changes under varying strains [[Figure 4B](#)]. Such a PEDOT:PSS-PVA hydrogel strain sensor demonstrates four linear fitting sections [[Figure 3J](#)], with GF of 2.15 in the strain range of 0%-100%, 3.63 for 100%-200%, 4.94 for 200%-250%, and 12.78 for 250%-300%, respectively.

To further validate the sensor's response to external stimuli, it was subjected to rapid loading and unloading cycles, showing instantaneous resistance changes within 330 ms [[Figure 4C](#)]. Additionally, the device's resistance to interference is tested at different frequencies (1-9 Hz), with no significant difference in relative resistance observed [[Figure 4D](#)]. This frequency-independent sensing behavior better ensures the accuracy and reliability of the sensor in plant growth monitoring. Additionally, to compare the sensing characteristics of the sensor under radial and lateral strains, we test its relative resistance changes in different directions. The experimental data indicates that our sensor shows no significant fluctuations in longitudinal resistance signals during lateral stretching, demonstrating its capability for precise data monitoring, as demonstrated in [Supplementary Figure 17](#). At the same time, the device also shows that non-axial deformations (e.g., hammering and manual twisting) do not trigger much interference to the sensing detection, demonstrating excellent insensitivity of our device against pressure and torsion disturbance [[Figure 4E](#) and [F](#)]. Furthermore, the sensor displays good long-term stability, with no significant drift in relative resistance after 3,000 loading and unloading cycles [[Figure 4G](#)] due to the seamless integration of the device. Compared to previously reported PEDOT:PSS-PVA strain sensors as depicted in [Supplementary Table 1](#)<sup>[50-53]</sup>, our fully 3D-printed device exhibits higher sensitivity over a wide strain range and stability under cyclic stretching. The measured factor is 12.78, demonstrating that the full 3D printing technique effectively improves the sensing device's performance while reducing tedious steps [[Figure 4H](#)]. Overall, the superior sensing properties of our 3D-printed strain sensing devices make them suitable for practical applications, such as plant growth monitoring.

### **Application of all-3D-printed strain sensors for plant growth monitoring**

Highly sensitive strain-sensing devices are used as measurement tools to visually analyze plant growth. In this work, an integrated PEDOT:PSS-PVA hydrogel strain-sensing device is carefully manufactured using 3D printing technology and attached to the stem of a plant to monitor its growth in real time and accurately. The device detects an increase in electrical resistance when subjected to external tensile forces, similar to the plant growth phenomenon. During plant growth, cells expand through division, which the

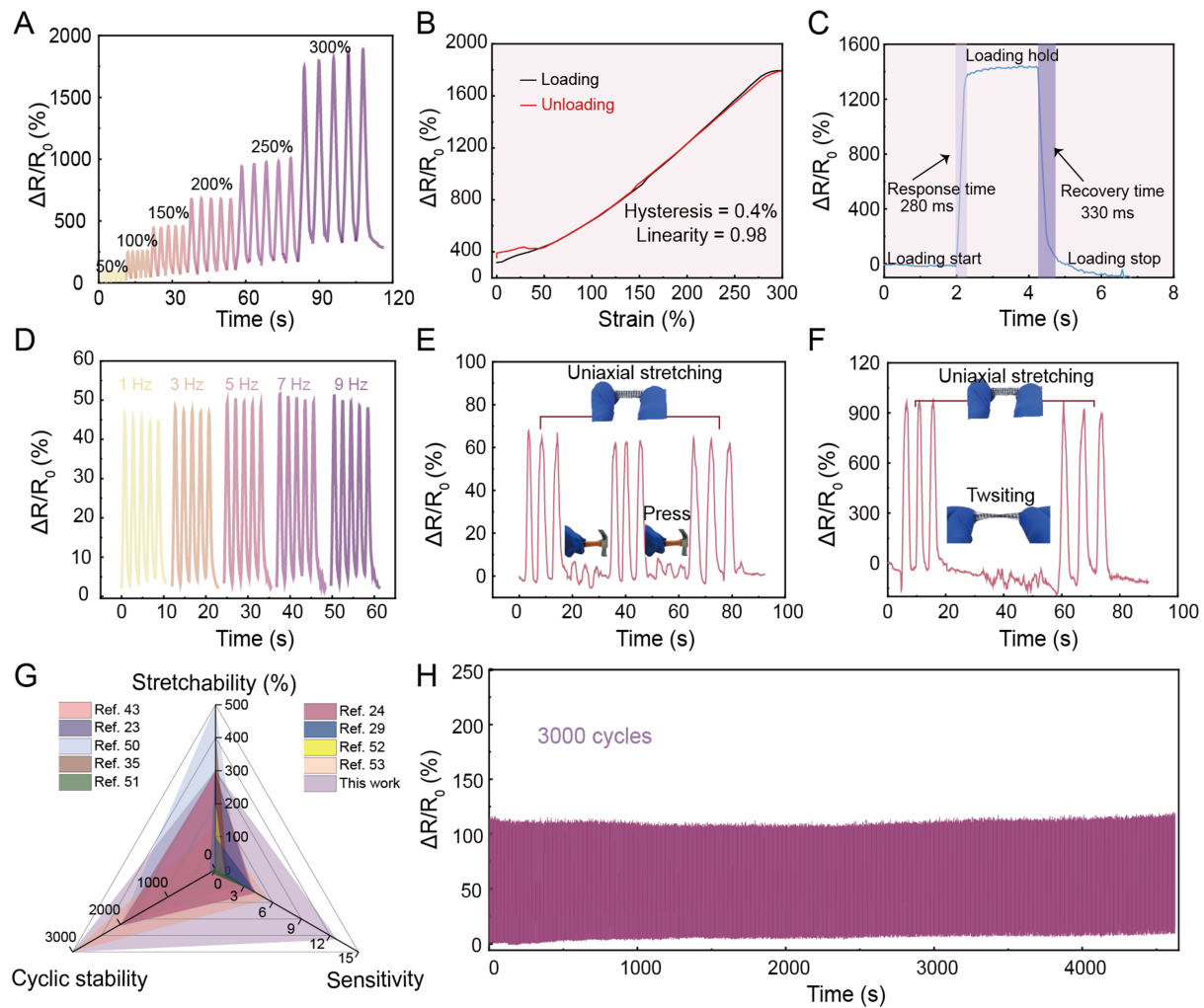


**Figure 4.** Sensing properties of the 3D printed PEDOT:PSS-PVA strain sensing device. (A) Relative resistance variation of the sensing devices at large strain (0%-300%); (B) The sensing device with linearity ( $R^2 = 0.98$ ) and hysteresis (0.4) within the 0%-300% strain range; (C) Response time of the sensing device at 0%-300% of a cyclic strain; (D) Change in relative resistance of this sensing device at different frequencies for the same time and strain conditions (50%); (E) Resistance to stress interference. The inset displays a sample of the device under uniaxial tension (~50%) and hammering, respectively; (F) Torsion resistance. The insets illustrate a sample of the device under uniaxial stretching (~250%) and manual torsion conditions, respectively; (G) Comparison of the performance of PEDOT:PSS-PVA-based strain sensing devices (stretchability, cyclic stability, and sensitivity); (H) Cycling stability at a strain of 100% within 3,000 cycles. PEDOT:PSS: Poly(3,4-ethylenedioxythiophene); polystyrene sulfonate; PVA: polyvinyl alcohol.

device senses as external deformation, aiding in understanding plant growth. To evaluate the performance of the strain-sensing device, a practical application was carried out. As demonstrated in [Figure 5A](#), the strain-sensing device was attached transversely and longitudinally to the bamboo to monitor its growth.

To further demonstrate the device's ability to detect subtle plant growth, we monitored growth in different dimensions. As shown in [Figure 5B](#) and [C](#), physical images of bamboo growing taller vertically and thickening horizontally were taken over 14 days. Notably, the 3D-printed strain-sensing device has good stretchability, accommodating the growth of different plant parts. To compare the sensing characteristics of the sensor under radial and lateral strains, we tested its relative resistance changes in different directions. Furthermore, we analyze the sensing performance parameters of the device to assess and calculate plant growth. Among these parameters, linearity is a measurement of the maximum deviation of the actual

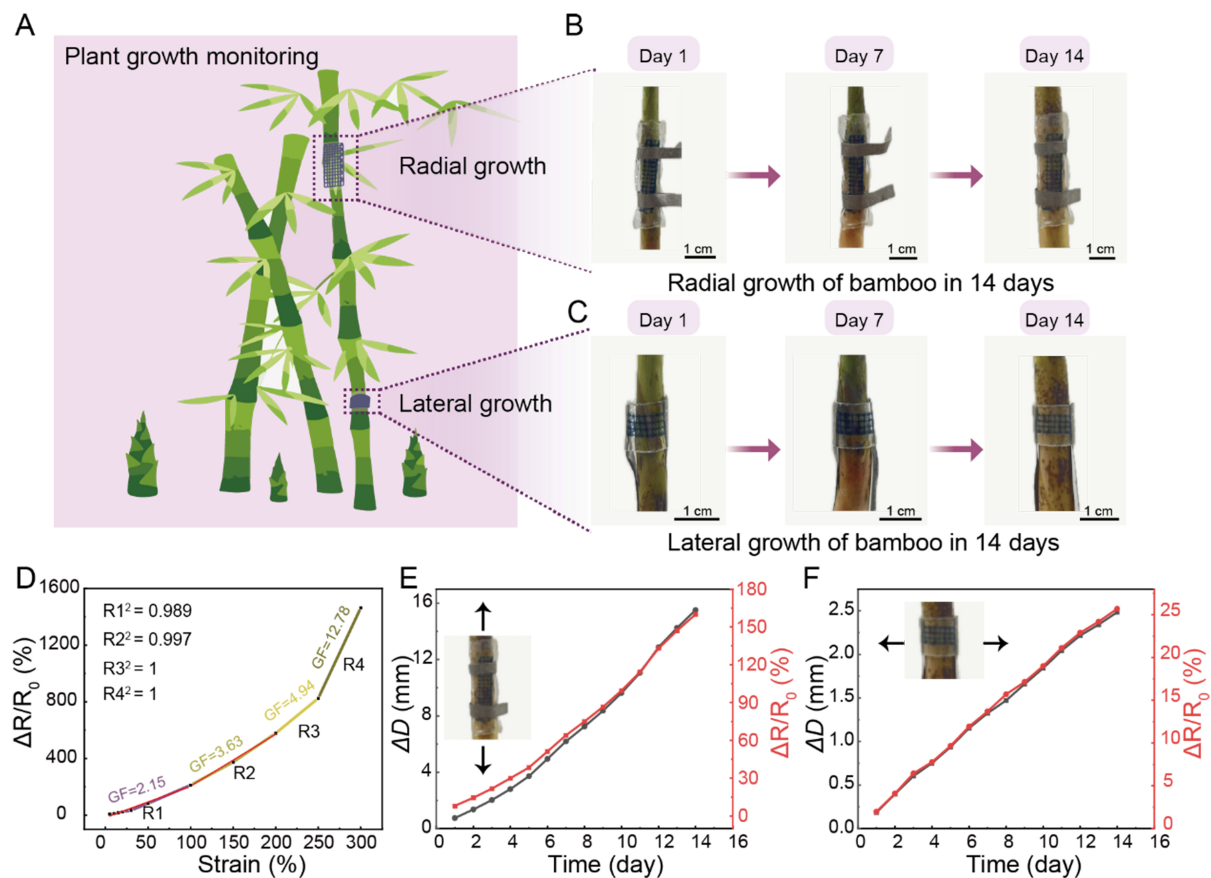


**Figure 5.** Application of 3D printed PEDOT:PSS-PVA strain sensing device for bamboo growth monitoring. (A) Scenario construction of strain sensing devices by all 3D printing for real-time tracking of bamboo growth; Physical drawings of the radial (B) and lateral (C) growth processes of bamboo on Day 1, Day 7, and Day 14; (D) Sensing characteristics of all-3D-printed strain sensing devices under the 0%-300% strain range (sensitivity and linearity); (E) Strain sensing device to monitor vertical growth of bamboo for 14 days; (F) Strain sensing device to monitor horizontal growth of bamboo for 14 days ( $\Delta D$ : Growth height of bamboo). PEDOT:PSS: Poly(3,4-ethylenedioxythiophene):polystyrene sulfonate; PVA: polyvinyl alcohol.

characteristic curve of the sensor from a theoretical straight line. When the  $R^2$  value approaches 1, it indicates that the sensor's theoretical values closely match the actual values. Remarkably, our integrally printed strain sensing device demonstrates excellent linearity across different strain ranges, showcasing its high practical application value [Figure 5D]. In plant growth detection, we utilize the resistance values and sensitivity of this sensing device across various strain ranges to infer plant height. This capability holds promise for monitoring the dynamic growth process of plants. Figure 5E and F indicates that the bamboo's growth rates in different dimensions vary, with vertical growth significantly faster than horizontal growth, consistent with the natural vertical growth pattern of bamboo. After 14 days of continuous monitoring, the bamboo grew at a rate of about 1 mm·day<sup>-1</sup> vertically and about 0.18 mm·day<sup>-1</sup> laterally. These experiments prove that our 3D-printed strain-sensing device displays a high sensitivity for detecting small growth changes in plants.

The high sensitivity of the strain-sensing device is due to the structural design of the sensing layer, which regulates the device's conductive pathway by 3D printing, thus increasing its sensitivity. This discovery not only provides a new and efficient 3D printing processing technology for integrated strain-sensing devices but also offers strong technical support for the intelligent development of agriculture.

## CONCLUSION

In this work, we present a novel all-3D-printed technology to fabricate customized, programmable, soft, and highly sensitive strain-sensing devices through continuous multi-material printing. Two viscoelastic inks have been characterized based on DIW 3D printing technique, and optimal printing parameters are selected to counteract solution diffusion behavior, ensuring high-fidelity printing. Additionally, sequentially designed and adapted printing modes enable the seamless fabrication of an integrated strain-sensing device. The performance and feasibility of the device are further comprehensively evaluated, including mechanical properties, electrical properties, and sensing signal analysis at different strains. The results indicate that the printed strain-sensing device exhibits superior tensile properties and higher sensitivity. The effectiveness of the sensing device has been demonstrated through real-time monitoring of plant growth. To achieve multi-channel monitoring of different plants, future research can be focused on developing a multi-channeled interconnected conductive pathway using multi-material 3D printing techniques. Overall, the proposed multi-material all-3D printing technique offers a promising platform for streamlined efficient fabrication of high-performance strain-sensing devices capable of real-time accurate monitoring of plant growth, potentially usable for plant sensing and related fields such as wearable devices, soft robots, and bioelectronics.

## DECLARATIONS

### Authors' contributions

Manuscript writing, 3D-printing fabrication, formal analysis, data curation, investigation, conceptualization: Wang, L.

Conceptualization, manuscript review, formal analysis: Wang, W.

Investigation, formal analysis, conceptualization: Wan, R.

3D-printing methodology, data curation, investigation: Yao, M.

3D-printing fabrication, data curation: Chen, W.

Data curation, investigation, conceptualization: Zhang, L.

Supervision, resources, funding acquisition: Xu, J.

Conceptualization, formal analysis, supervision, resources: Liu, X.

Conceptualization, writing - review and editing, data curation, supervision, resources, funding acquisition: Lu, B.

### Availability of data and materials

The raw data supporting the findings of this study are available within this Article and its [Supplementary Materials](#). Further data are available from the corresponding authors upon request.

### Financial support and sponsorship

This work was supported by the National Natural Science Foundation of China (52373184 & 52473179), the Key Research and Development Program of Jiangxi Province (20223BBE51023), the Natural Science Foundation of Jiangxi Province (20232ACB204002 & 20232BAB202044), and the Jiangxi Provincial Key Laboratory of Flexible Electronics (20212BCD42004 & 20242BCC32010).

### Conflicts of interest

All authors declared that there are no conflicts of interest.

### Ethical approval and consent to participate

Not applicable.

## Consent for publication

Not applicable.

## Copyright

© The Author(s) 2025.

## REFERENCES

1. Lee, H. J.; Joyce, R.; Lee, J. Liquid polymer/metallic salt-based stretchable strain sensor to evaluate fruit growth. *ACS. Appl. Mater. Interfaces.* **2022**, *14*, 5983-94. [DOI](#) [PubMed](#)
2. Nagelmüller, S.; Kirchgessner, N.; Yates, S.; Hiltbold, M.; Walter, A. Leaf length tracker: a novel approach to analyse leaf elongation close to the thermal limit of growth in the field. *J. Exp. Bot.* **2016**, *67*, 1897-906. [DOI](#) [PubMed](#) [PMC](#)
3. Li, S.; Wang, H.; Ma, W.; et al. Monitoring blood pressure and cardiac function without positioning via a deep learning-assisted strain sensor array. *Sci. Adv.* **2023**, *9*, eadh0615. [DOI](#) [PubMed](#) [PMC](#)
4. Gong, T.; Zhang, H.; Huang, W.; et al. Highly responsive flexible strain sensor using polystyrene nanoparticle doped reduced graphene oxide for human health monitoring. *Carbon* **2018**, *140*, 286-95. [DOI](#)
5. Li, J.; Ding, Q.; Wang, H.; et al. Engineering smart composite hydrogels for wearable disease monitoring. *Nanomicro. Lett.* **2023**, *15*, 105. [DOI](#) [PubMed](#) [PMC](#)
6. Zhang, Z.; Chen, G.; Xue, Y.; et al. Fatigue-resistant conducting polymer hydrogels as strain sensor for underwater robotics. *Adv. Funct. Mater.* **2023**, *33*, 2305705. [DOI](#)
7. Yang, D.; Feng, M.; Gu, G. High-stroke, high-output-force, fabric-lattice artificial muscles for soft robots. *Adv. Mater.* **2024**, *36*, e2306928. [DOI](#)
8. Li, J.; Cao, J.; Lu, B.; Gu, G. 3D-printed PEDOT:PSS for soft robotics. *Nat. Rev. Mater.* **2023**, *8*, 604-22. [DOI](#)
9. Yoon, H.; Ha, H.; Choi, C.; Yun, T. G.; Hwang, B. Mini review on PEDOT:PSS as a conducting material in energy harvesting and storage devices applications. *J. Polym. Mater.* **2023**, *40*, 1-17. [DOI](#)
10. Sudhahar, S.; G, U.; Alla, J. P.; Jonnalagadda, R. R.; Lakshmi, S.; Gupta, S. Acrylic finished leather upgraded with thermoplastic polyurethane filament using 3D printing - a new generation hybrid leather of synthetic and natural polymer. *J. Polym. Mater.* **2023**, *40*, 33-45. [DOI](#)
11. Shen, Z.; Liu, F.; Huang, S.; et al. Progress of flexible strain sensors for physiological signal monitoring. *Biosens. Bioelectron.* **2022**, *211*, 114298. [DOI](#)
12. Lin, J.; Chen, X.; Zhang, P.; et al. Wireless bioelectronics for in vivo pressure monitoring with mechanically-compliant hydrogel biointerfaces. *Adv. Mater.* **2024**, *36*, 2400181. [DOI](#)
13. Wan, R.; Yu, J.; Quan, Z.; et al. A reusable, healable, and biocompatible PEDOT:PSS hydrogel-based electrical bioadhesive interface for high-resolution electromyography monitoring and time-frequency analysis. *Chem. Eng. J.* **2024**, *490*, 151454. [DOI](#)
14. Ke, X.; Mu, X.; Chen, S.; et al. Reduced graphene oxide reinforced PDA-Gly-PVA composite hydrogel as strain sensors for monitoring human motion. *Soft. Sci.* **2023**, *3*, 21. [DOI](#)
15. Yao, X.; Zhang, S.; Qian, L.; et al. Super stretchable, self-healing, adhesive ionic conductive hydrogels based on tailor-made ionic liquid for high-performance strain sensors. *Adv. Funct. Mater.* **2022**, *32*, 2204565. [DOI](#)
16. Zhu, H.; Hu, X.; Liu, B.; Chen, Z.; Qu, S. 3D printing of conductive hydrogel-elastomer hybrids for stretchable electronics. *ACS. Appl. Mater. Interfaces.* **2021**, *13*, 59243-51. [DOI](#) [PubMed](#)
17. Yang, J.; Cheng, J.; Qi, G.; Wang, B. Ultrastretchable, multihealable, and highly sensitive strain sensor based on a double cross-linked MXene hydrogel. *ACS. Appl. Mater. Interfaces.* **2023**, *15*, 17163-74. [DOI](#)
18. Wang, F.; Xue, Y.; Chen, X.; et al. 3D printed implantable hydrogel bioelectronics for electrophysiological monitoring and electrical modulation. *Adv. Funct. Mater.* **2024**, *34*, 2314471. [DOI](#)
19. Su, X.; Wu, X.; Chen, S.; et al. A highly conducting polymer for self-healable, printable, and stretchable organic electrochemical transistor arrays and near hysteresis-free soft tactile sensors. *Adv. Mater.* **2022**, *34*, e2200682. [DOI](#)
20. Wei, J.; Zheng, Y.; Chen, T. A fully hydrophobic ionogel enables highly efficient wearable underwater sensors and communicators. *Mater. Horiz.* **2021**, *8*, 2761-70. [DOI](#)
21. Xiong, Y.; Lin, Z.; Zhao, Z.; et al. A template-stripped carbon nanofiber/poly(styrene-butadiene-styrene) compound for high-sensitivity pressure and strain sensing. *Soft. Sci.* **2022**, *2*, 14. [DOI](#)
22. Zhang, J.; Wang, M.; Yang, Z.; Zhang, X. Highly flexible and stretchable strain sensors based on conductive whisker carbon nanotube films. *Carbon* **2021**, *176*, 139-47. [DOI](#)
23. Park, H.; Kim, D. S.; Hong, S. Y.; et al. A skin-integrated transparent and stretchable strain sensor with interactive color-changing electrochromic displays. *Nanoscale* **2017**, *9*, 7631-40. [DOI](#)
24. Abed, A.; Samouh, Z.; Cochrane, C.; et al. Piezo-resistive properties of bio-based sensor yarn made with sisal fibre. *Sensors* **2021**, *21*, 4083. [DOI](#) [PubMed](#) [PMC](#)
25. Wu, Z.; Zhao, Q.; Luo, X.; et al. Low-cost fabrication of high-performance fluorinated polythiophene-based vis-NIR electrochromic devices toward deformable display and camouflage. *Chem. Mater.* **2022**, *34*, 9923-33. [DOI](#)

26. Xie, H.; Huang, Z.; Wan, J.; et al. Dual-band laser selective etching for stretchable and strain interference-free pressure sensor arrays. *Adv. Funct. Mater.* **2024**, *34*, 2401532. DOI
27. Yue, Y.; Li, X.; Zhao, Z.; Wang, H.; Guo, X. Stretchable flexible sensors for smart tires based on laser-induced graphene technology. *Soft. Sci.* **2023**, *3*, 13. DOI
28. Agarwala, S.; Goh, G. L.; Dinh, L. T. S.; et al. Wearable bandage-based strain sensor for home healthcare: combining 3D aerosol jet printing and laser sintering. *ACS. Sens.* **2019**, *4*, 218-26. DOI
29. Shi, W.; Wang, Z.; Song, H.; et al. High-sensitivity and extreme environment-resistant sensors based on PEDOT:PSS@PVA hydrogel fibers for physiological monitoring. *ACS. Appl. Mater. Interfaces.* **2022**, *14*, 35114-25. DOI
30. Li, C.; Cheng, J.; He, Y.; et al. Polyelectrolyte elastomer-based ionotronic sensors with multi-mode sensing capabilities via multi-material 3D printing. *Nat. Commun.* **2023**, *14*, 4853. DOI PubMed PMC
31. Cheng, J.; Wang, R.; Sun, Z.; et al. Centrifugal multimaterial 3D printing of multifunctional heterogeneous objects. *Nat. Commun.* **2022**, *13*, 7931. DOI PubMed PMC
32. Zeng, S.; Zhang, J.; Zu, G.; Huang, J. Transparent, flexible, and multifunctional starch-based double-network hydrogels as high-performance wearable electronics. *Carbohydr. Polym.* **2021**, *267*, 118198. DOI PubMed
33. Xia, S.; Zhang, Q.; Song, S.; Duan, L.; Gao, G. Bioinspired dynamic cross-linking hydrogel sensors with skin-like strain and pressure sensing behaviors. *Chem. Mater.* **2019**, *31*, 9522-31. DOI
34. Wang, Q.; Liu, J.; Ran, X.; Zhang, D.; Shen, G.; Miao, M. High-performance flexible self-powered strain sensor based on carbon nanotube/ZnSe/CoSe<sub>2</sub> nanocomposite film electrodes. *Nano. Res.* **2022**, *15*, 170-8. DOI
35. Zhao, W.; Zhang, D.; Yang, Y.; Du, C.; Zhang, B. A fast self-healing multifunctional polyvinyl alcohol nano-organic composite hydrogel as a building block for highly sensitive strain/pressure sensors. *J. Mater. Chem. A.* **2021**, *9*, 22082-94. DOI
36. Xia, X.; Xiang, Z.; Gao, Z.; et al. Structural design and DLP 3D printing preparation of high strain stable flexible pressure sensors. *Adv. Sci.* **2024**, *11*, e2304409. DOI PubMed PMC
37. Poompiet, N.; Pattanapun, P.; Aumnate, C.; Román, A. J.; Osswald, T. A.; Potiyaraj, P. 3D printable resin/carbon nanotube composites for wearable strain sensors: enhancing mechanical and electrical properties. *J. Sci. Adv. Mater. Dev.* **2023**, *8*, 100546. DOI
38. Han, S.; Wu, Q.; Xu, Y.; et al. Multi-functional eutectic hydrogel for 3D printable flexible omnidirectional strain sensors. *Adv. Mater. Technol.* **2023**, *8*, 2301123. DOI
39. Guo, B.; Zhong, Y.; Chen, X.; Yu, S.; Bai, J. 3D printing of electrically conductive and degradable hydrogel for epidermal strain sensor. *Compos. Commun.* **2023**, *37*, 101454. DOI
40. Zhang, C.; Zheng, H.; Sun, J.; et al. 3D printed, solid-state conductive ionoelastomer as a generic building block for tactile applications. *Adv. Mater.* **2022**, *34*, e2105996. DOI PubMed
41. Ertugrul, I.; Ulkir, O.; Ersoy, S.; Ragulskis, M. Additive manufactured strain sensor using stereolithography method with photopolymer material. *Polymers* **2023**, *15*, 991. DOI PubMed PMC
42. Sanandiy, N. D.; Pai, A. R.; Seyedin, S.; Tang, F.; Thomas, S.; Xie, F. Chitosan-based electroconductive inks without chemical reaction for cost-effective and versatile 3D printing for electromagnetic interference (EMI) shielding and strain-sensing applications. *Carbohydr. Polym.* **2024**, *337*, 122161. DOI PubMed
43. Christ, J. F.; Aliheidari, N.; Ameli, A.; Pötschke, P. 3D printed highly elastic strain sensors of multiwalled carbon nanotube/thermoplastic polyurethane nanocomposites. *Mater. Design.* **2017**, *131*, 394-401. DOI
44. Liu, Z.; Cai, M.; Hong, S.; et al. Data-driven inverse design of flexible pressure sensors. *Proc. Natl. Acad. Sci. U. S. A.* **2024**, *121*, e2320222121. DOI PubMed PMC
45. Jiang, Y.; Liu, Z.; Matsuhisa, N.; et al. Auxetic mechanical metamaterials to enhance sensitivity of stretchable strain sensors. *Adv. Mater.* **2018**, *30*, e1706589. DOI
46. Yuk, H.; Lu, B.; Lin, S.; et al. 3D printing of conducting polymers. *Nat. Commun.* **2020**, *11*, 1604. DOI PubMed PMC
47. Shen, Z.; Zhang, Z.; Zhang, N.; et al. High-stretchability, ultralow-hysteresis conductingpolymer hydrogel strain sensors for soft machines. *Adv. Mater.* **2022**, *34*, e2203650. DOI
48. Cao, J.; Zhang, Z.; Li, K.; et al. Self-healable PEDOT:PSS-PVA nanocomposite hydrogel strain sensor for human motion monitoring. *Nanomaterials* **2023**, *13*, 2465. DOI PubMed PMC
49. Yang, R.; Tu, Z.; Chen, X.; Wu, X. Highly stretchable, robust, sensitive and wearable strain sensors based on mesh-structured conductive hydrogels. *Chem. Eng. J.* **2024**, *480*, 148228. DOI
50. Peng, X.; Wang, W.; Yang, W.; et al. Stretchable, compressible, and conductive hydrogel for sensitive wearable soft sensors. *J. Colloid. Interface. Sci.* **2022**, *618*, 111-20. DOI
51. Peng, Y.; Pi, M.; Zhang, X.; et al. High strength, antifreeze, and moisturizing conductive hydrogel for human-motion detection. *Polymer* **2020**, *196*, 122469. DOI
52. Gong, J.; Sun, F.; Pan, Y.; et al. Stretchable and tough PAANA/PEDOT:PSS/PVA conductive hydrogels for flexible strain sensors. *Mater. Today. Commun.* **2022**, *33*, 104324. DOI
53. Zhang, Y.; Guo, M.; Zhang, Y.; et al. Flexible, stretchable and conductive PVA/PEDOT:PSS composite hydrogels prepared by SIPN strategy. *Polym. Test.* **2020**, *81*, 106213. DOI